Effects of electrical parameters on plasma electrolytic oxidation of aluminium

J. Martin, A. Melhem, I. Shchedrina, T. Duchanoy, A. Nominé, G. Henrion, T. Czerwiec, T. Belmonte

Effects of electrical parameters on plasma electrolytic oxidation of aluminium

J. Martin[1,*], A. Melhem[1], I. Shchedrina[1,2], T. Duchanoy[1], A. Nominé[1,2], G. Henrion[1], T. Czerwiec[1], and T. Belmonte[1]

[1] Université de Lorraine, UMR CNRS 7198, Institut Jean Lamour – Département Chimie et Physique des Solides et des Surfaces, Parc de Saurupt – CS 50840, F-54011 Nancy cedex (France)

[2] National University of Science and Technology «MISIS», Department of Metal Protection and Surface Engineering, Leninsky prospect 4, 119049, Moscow (Russian Federation)

*Corresponding author: Tel.: +33 383 584 251

julien.martin@univ-lorraine.fr,

The plasma electrolytic oxidation (PEO) of aluminium alloys is investigated for different electrical working conditions using a pulsed bipolar current supply. A particular attention is paid to the effect of the anodic current density (from 10 to 90 $A.dm^{-2}$) and current pulse frequency (from 100 to 900 Hz) on the resulting oxide layer. Micro-discharges are characterized during the process by means of fast video imaging with a time and a space resolution of 8µs and 0.017 mm^2, respectively. Correlations are established between the micro-discharge characteristics (surface density, lifetime and size) and the elaborated oxide layers (morphology, growth rate and surface roughness). The highest coating growth rate measured (2.1 $\mu m.min^{-1}$) is achieved with the combination of the highest current density (75.7 $A.dm^{-2}$) and the highest current pulse frequency (900 Hz). Within these specific current conditions it is concluded that the detrimental effects of numerous micro-discharges are minimized. Results also show that the surface roughness may be largely affected by the

presence of long-lived and large micro-discharges which develop over the processed surface. The strongest micro-discharges (live duration up to 0.3 ms and cross-sectional area up to 1 mm^2) are mainly observed with the combination of the highest current density (75.7 $A.dm^{-2}$) and the lowest current pulse frequency (100 Hz).

Keywords

Plasma Electrolytic Oxidation (PEO), Micro-Arc Oxidation (MAO), Pulsed bipolar current, Aluminium, Fast-video imaging, Micro-discharge

1.0 Introduction

Plasma Electrolytic Oxidation (PEO), also known as Micro-Arc Oxidation (MAO) is a particular technique to produce oxide ceramic coatings on light-weight valve metals (such as Al, Mg, Zr, Ti and their alloys). Growth of the oxide layer takes place at potentials above the dielectric breakdown voltage of the insulating oxide surface layer resulting in the development of a large number of short-lived micro-discharges (MDs) which move randomly over the processed surface [1-3]. The resulting coating exhibits improved surface performances in terms of hardness, wear protection and corrosion resistance [4-7]. Associated with the use of environmentally friendly diluted alkaline electrolytes, PEO process gains a growing interest in various industrial domains (transport, energy, medicine) to replace conventional chromic acid anodizing (CAA) or hard acid anodizing (HAA) [2, 8].

Numerous studies on the growth mechanisms of PEO coatings have been carried out. All evidence the key role played by the MDs. Plasma during the PEO process has been investigated by using optical emission spectroscopy [9-13]. In this field, Konjević's research group report several studies on the determination of the electron number densities N_e and electron temperature T_e in real time with the PEO process [14-17]. MDs have also been studied by video imaging in order to determine their surface number density, lifetime and size at different stages of the treatment. Yerokhin *et al.* [18] recorded video images at 24 Hz (41 ms time resolution) when AC PEO processing of aluminium samples. Matykina *et al.* [19] observed the MDs on titanium with a time resolution of 10 ms, while Mécuson *et al.* [20] studied the MDs behaviour during bipolar pulse PEO of aluminium using an exposure time of 2 ms. More recently, Melhem *et al.* [21, 22] demonstrated the necessity of improving the time resolution to the microsecond range in order to get a more reliable estimation of the MDs characteristics.

In the present work, MDs were examined during the bipolar pulse PEO treatment of Al alloys using fast-video imaging with a time resolution of 8 µs. Measurements allowed us to

investigate the influence of the imposed bipolar current pulse on processed materials. A particular attention was paid to the current density and the current pulse frequency values which are known to have strong effects on the performances of the grown oxide layers [23, 24]. The latter were characterized by roughness measurements and by scanning electron microscopy observations of both the top surface and coating cross sections. An attempt is made to draw close correlations between measurements on the MDs and material characteristics to better understand the growing mechanisms of the protective coatings.

2.0 Experimental procedure

The experimental set-up consists basically of an electrolysis tank containing an electrolytic solution made of KOH and Na_2SiO_3 diluted in distilled water in the range of 1 $g.l^{-1}$. A cooling device allows us to maintain the temperature of the electrolytic solution below 30 °C (303 K) during the process. The electrolyte electrical conductivity and pH are 2.8 $mS.cm^{-1}$ and 13, respectively. Two rectangular titanium counter-electrodes (cathodes) face both sides of the sample (anode). The electrode gap between each counter-electrode and the sample is 28.5 mm. A bipolar current pulse generator (Ceratronic® process [25]) working in galvanostatic mode is used to supply both the sample and the counter-electrodes. As reported by Mécuson *et al.*, different shapes of the applied current waveform can be achieved by adjusting the current parameters (rising and fall time, frequency, amplitude, offset) over a wide range of values [10, 11, 20]. So, the amplitude of the positive (I_p) and negative (I_n) currents, the current pulse frequency (F) and the anodic to cathodic charge quantity ratio ($R = Q_p/Q_n$) can be adjusted to suitable values [20]. In particular, they established that applying a higher negative charge quantity than the positive one (R = 0.89 hereinafter referred to as "soft" regime) to the Al alloy sample greatly improves the resulting oxide layer properties by reducing the detrimental effects of strong arc discharges. With this particular soft regime conditions, the positive current density (J_p) and current pulse frequency (F) are investigated in the range 10 to 90 $A.dm^{-2}$ and 100 to 1000 Hz, respectively. Two grades of Al alloys were

used as substrate in this work. The effect of the positive current density was investigated using 2214 grade Al alloy while 1050 grade Al alloy was used to study the effects of the current pulse frequency. The chemical composition of both Al alloys is given in table 1. Samples have a rectangular shape of 50 mm × 30 mm × 6 mm. Prior to be processed, samples are polished with 320 grit SiC abrasive papers, ultrasonically cleaned with acetone and dried. Samples in 2214 grade Al alloy were processed for 70 min while samples in 1050 grade Al alloy were treated for 40 min.

Video images of the MDs during PEO processing are recorded using a Photron SA1.1 camera which allows us to study the MDs evolution either along the current period or over the processing time. For the present study, the sampling rate is set at 125 000 frames per second (125 kfps) which corresponds to a time resolution of 8 µs. Under these specific recording conditions, the spatial resolution of the camera was set at 0.017 mm^2 which is much lower (by a factor of ~15) than the minimum area of MDs that was detected in the experiments. Automatic image processing is done using an homemade software [26, 27] allowing us to follow the MDs surface number density per unit time, the lifetime (ms) and the size (area in mm^2) distributions of the MDs on the surface as a function of the processing time.

Top views and cross-sections of the PEO-treated samples were examined by field emission gun scanning electron microscopy (FEG-SEM - Philips XL30) working in backscattered electron mode. Prior to be examined, samples were cut, mounted in resin, polished through successive grades of SiC abrasive papers and finely polished to 1 µm with diamond paste. The centre and the edge of the treated samples were closely examined. The centre of the sample is defined as an investigated area (2 mm × 2 mm) centred at the intersection of the two diagonals of the rectangular shape of the sample. Concerning the edge of the sample, the investigated area (2 mm × 2 mm) is located at 1 mm from the center of its longest side. In both regions, the coating thickness was determined as the average value of 20 measures taken on cross-section over 20 different positions (each 100 µm). The average mean surface roughness of the

coating, R_a (µm), was assessed using a Surfscan 3S profilometer with lateral and depth resolutions of 8 µm and 0.1 µm, respectively. Roughness of the samples before PEO treatment is 0.20 µm.

3.0 Experimental results and discussion

3.1 Establishment of the "soft" sparking regime

In our previous studies, it was established that setting the anodic to cathodic charge quantity ratio R less than 1 leads to a total modification of the growth regime that switches from an "arcs" regime to a "softer" one [20, 21]. The latter does not exhibit the strong arcs that were reported as detrimental to the oxide layer properties thus resulting in thicker, more dense and more homogeneous (in terms of thickness over the sample area) layers. The "arcs" to "soft" regime switching time is detected by the drop in the anodic voltage amplitude (Fig. 1) due to the change in the impedance of the substrate/layer system [20, 28]. The dependence of the switching time on the anodic current density and current pulse frequency is plotted in figure 2a and figure 2b respectively. The higher the current density and the current pulse frequency, the earlier the process switches to "soft" regime. Transition appears at 62 min with 25.2 $A.dm^{-2}$ at 100 Hz and drops to 14 min with 75.7 $A.dm^{-2}$ at 900 Hz. It is also worth noting that after 100 min of treatment with the lowest investigated current density (12.5 $A.dm^{-2}$) and pulse frequency (100 Hz), the "soft" regime is not reached.

3.2 Micro-discharges characteristics

Figure 3 shows the spatial distribution of the MDs over the sample surface (at 75.5 $A.dm^{-2}$ and 100 Hz electrical conditions) at various processing time (1, 5, 10 and 15 min). Each plot consists of an integration of the 11 250 processed images over 9 periods of the current periods (90 ms). It clearly appears that the number of MDs which develop over the surface decreases progressively as the PEO process time increases. Moreover, at the beginning of the PEO treatment (especially before 5 min treatment time), the MDs do not cover the sample surface uniformly. Indeed, a large amount of MDs are preferentially located at the corners and at the

edges of the sample. Such kind of non-uniformity of the PEO treatment has already been reported by by Melhem *et al.* [21] within similar processing conditions.

Figure 4 shows the evolution of the surface number density of MDs determined by means of video-imaging as a function of the PEO processing time for the different anodic current densities (Fig. 4a) and current pulse frequencies that were investigated (Fig. 4b). Whatever the electrical conditions used MDs surface density at the beginning of the process (after 1 min treatment time) is higher than 5.10^5 $cm^{-2}.s^{-1}$. As the PEO process goes on, the surface density of MDs decreases nearer to 10^4 $cm^{-2}.s^{-1}$ at longer treatment times (up to 50 min). The decrease is much stronger as the current density and the current frequency get higher. It is worth noting that with the specific electrical conditions, (12.6 $A.dm^{-2}$; 100 Hz), the process does not switch to the soft regime. Consequently, the surface density of MDs remains quite high, (~1.10^5 $cm^{-2}.s^{-1}$) even at long treatment times.

The fitting of the experimental data points using a double exponential decay law (solid line in figure 4a) clearly points out that the decay of the MDs number on the surface results from two distinct phenomena which are likely due to the breakdown mechanisms and consequently to the layer thickness and dielectric properties. However, further works are needed to clearly identify these mechanisms.

The lifetime distributions of MDs were determined for the various electrical conditions investigated. Such distributions recorded at 10 min processing time and before the establishment of the “soft” sparking regime are plotted in figure 5. It shows the surface density of MDs as a function of the MDS life-time. Integration of this distribution curve allows us to determine the arithmetic average of the MDs life-time. Irrespective of the applied electrical conditions, most of the MDs last less than 200 µs. The MDs lifetime increases with the increase in the current density with an average duration of ~21, ~41 and ~56 µs at 12.6, 37.9 and 63.1 $A.dm^{-2}$, respectively. Long-lived MDs are observed at high current density. The lifetime of MDs decreases with increasing the current pulse frequency with an average

duration of ~49, ~47, and ~38 µs at 100, 500 and 900 Hz, respectively. Long–lived MDs are produced at low frequencies.

Figure 6 is the distribution in size of MDs recorded at 10 min processing time for three different current density values (Fig. 6a) and three different pulse frequencies (Fig. 6b). It shows the surface density of MDs as a function of the MDs size. It can be seen that whatever the processing conditions used a large amount of MDs exhibits a small size (area) between 0.5 and 1 mm^2. Figure 6a illustrates the influence of the current density on the size distribution of MDs. It shows that the large MDs are promoted at high current density. The arithmetic average size calculated from the integration of the size distribution curve is about ~0.54 mm^2, ~0.72 mm^2 and ~0.76 mm^2 at 12.6, 37.9 and 63.1 $A.dm^{-2}$, respectively. At very low current density (12.6 $A.dm^{-2}$) size of the MDs doesn't exceed 2.0 mm^2. Figure 6b illustrates the effect of the current pulse frequency on the size distribution of MDs. It can be seen that size of the MDs tends to decrease with increasing the current pulse frequency with an average size of ~0.77 mm^2, ~0.63 mm^2 and ~0.56 mm^2 at 100, 500 and 900 Hz, respectively. Large size MDs are promoted when working at low current pulse frequencies.

3.3 Discussion about the elaborated oxide layers characteristics

Figures 7a-f show scanning electron microscopy micrographs of cross-section of PEO layers achieved within different electrical conditions. Micrographs in figures 7a-b were taken at the centre (Fig. 7a) and at the edge (Fig. 7b) of Al2214 sample processed for 100 min at low current density (12.6 $A.dm^{-2}$) and low current pulse frequency (100 Hz). Whatever the location on sample, the oxide layer consists of plates and appears as non-homogeneous with an irregular metal-oxide interface. It is rather thin with large porosities. This morphology, which is characteristic of a PEO discharge regime made of "arcs", can be explained by the fact that no transition from "arcs" to "soft" regime was observed for these specific electrical conditions (see Fig. 2a). Jaspard-Mécuson *et al.* [20] demonstrated that under "arcs" regime, such thin and damaged coating results from a competition between oxidation and erosion

mechanisms which are both assisted by numerous arc discharges. This is consistent with our previous observations regarding the surface number density of MDs which remains high even after long treatment duration for these specific conditions (Fig. 4a). Figures 7c-d show micrographs of Al1050 sample treated for 40 min at high current density 75.5 $A.dm^{-2}$ and low current pulse frequency (100 Hz). Observations were done at the centre (Fig. 7c) and at the edge (Fig. 7d) of the sample. Whatever the location on sample, micrographs evidence that increasing the anodic current density improves the coating thickness and morphology. This trend is closely connected to the "arcs" to "soft" regime transition which occurs earlier with higher current density leading to an earlier decrease in the MDs surface number density (Fig. 4a). The oxide layer thus elaborated is typical of a PEO treatment under "soft" regime conditions and can be divided into two sub-layers as described in the literature: an outer layer constituted of fine pores and an inner, more compact layer [10, 20]. Figures 7c-d also illustrate that the oxide layer in the centre (Fig. 7c) and in the edge (Fig. 7d) of the sample exhibit different morphology. Thickness of the oxide layer is thicker at the edge than at the centre. Homogeneity of the thickness is also improved at the edges than at the centre where it can be observed some residual large discharge channels and a plate-like layer at the top surface. This variation in the oxide layer morphology is related to the spatial gradient in the MDs number observed previously in the figure 3. At the edge, where MDs are numerous at the beginning of the PEO treatment, oxide layer is thicker and more compact than at the centre where less numerous MDs have been observed. Influence of the current pulse frequency on the oxide layer morphology is illustrated in figures 7e-f that show cross-sections of Al1050 sample processed for 40 min at high current pulse frequency 900 Hz at the centre (Fig. 7e) and at the edge (Fig. 7f). It can be clearly seen that the coatings become thicker and more compact as the working frequency increases which matches the earlier occurrence of the "soft" PEO treatment regime (Fig. 4). It is also accompanied by a more regular oxide layer/substrate interface and a more homogeneous treatment over the sample surface.

The average coating growth rate of the PEO coatings determined under different current densities and different current pulse frequencies is presented in figure 8a and 8b, respectively. Such average growth rate is calculated by dividing the final layer thickness by the treatment time. In the range of the investigated electrical conditions, the current density seems to have a more pronounced influence on the growth rate than the current pulse frequency parameter. It is also noteworthy that there is an enhancement of the average growth rate with the increase in both the current density and the current pulse frequency. For example, the highest coating growth rate observed (2.1 $\mu m.min^{-1}$) is achieved with the combination of the highest current density (75.7 $A.dm^{-2}$) and the highest current pulse frequency (900 Hz). In contrast, the lowest oxidation kinetics is attributed to the lowest current density (12.5 $A.dm^{-2}$) and the lowest current pulse frequency (100 Hz). This result is closely correlated to the MDs which become less numerous earlier and earlier as the surface is processed for higher current densities and higher current pulse frequencies. This promotes the occurrence of the "soft" regime transition as described above (Fig. 2 and 4). Figures 8a and 8b also illustrate another interesting feature: irrespective of the electrical conditions used, the average growth kinetics is always higher at the edge of the sample than at the centre. Nevertheless, it can be noted that this spatial gradient in the coating growth rate is more pronounced when working with high current density and low current pulse frequency.

Figure 9 reports on the dependence of the surface roughness of the oxide layers on the current density (Fig. 9a) and current pulse frequency (Fig. 9b). Figure 9a shows that roughness increases with the increase in current density while figure 9b evidences a decrease in roughness with the increase in current pulse frequency. This dependence can be associated with the strength of the MDs in terms of lifetime and size as discussed above which exhibits a similar tendency: MDs last longer and are larger for both higher current density and lower current pulse frequency. Roughness may be at least partly a consequence of the long-lived and large size MDs which have detrimental effects on the growing oxide surface. Within the

electrical conditions used, figure 9 shows that roughness measurements exhibit differences between the centre and the edge of the treated samples. Roughness is always higher at the edge of the sample than at the centre. Moreover, such spatial gradient in the roughness is stronger at high current density and low current pulse frequency.

4.0 Conclusion

In this study, the effects of the anodic current density (from 10 to 80 $A.dm^{-2}$) and the current pulse frequency (from 100 to 900 Hz) on the resulting oxide layer in the bipolar PEO processing of aluminium alloys have been investigated. Correlations between the micro-discharges characteristics (surface density, lifetime and size) and the processed material (thickness, homogeneity and roughness) have been discussed.

- Firstly, results show that fast-video imaging with a time resolution of 8 µs makes it possible to accurately investigate the micro-discharges in real-time over the PEO process.
- Secondly, it has been found that the increase in the anodic current density and the pulse frequency provides a qualitative improvement in the coating growth rate and homogeneity. This is explained by the surface number density of micro-discharges which falls down more rapidly with higher current density and higher frequency, leading to an earlier "soft" regime occurrence.
- Thirdly, results evidence that long-lived and large size micro-discharges (up to 0.3 ms and 1 mm^2, respectively) observed for high current density and low current pulse frequency are detrimental to the oxide layer roughness. On the contrary, short-lived and small size micro-discharges (down to 0.2 ms and 0.5 mm^2, respectively) measured at low current densities and high pulse frequency appears to have less detrimental effect on the material roughness.
- Finally, within the PEO process parameters investigated, our results indicate a spatial heterogeneity in morphology over the PEO processed sample area which becomes more

pronounced at high current density and low current pulse frequency. Average growth rate and roughness are higher at the edge than at the centre of the samples.

Acknowledgments

Financial support of the European Commission under grant agreement n° 270589 is greatly acknowledged. We also greatly acknowledge financial support from the Conseil Régional de Lorraine for granting A. Nominé's PhD work.

List of references

[1] P. Kurze, W. Krysmann, H.G. Schneider, Cryst. Res. Technol. 21 (1986) 1603-1609.

[2] A.L. Yerokhin, X. Nie, A. Leyland, A. Matthews, S.J. Dowey, Surf. Coat. Technol. 122 (1999) 73-93.

[3] F. Monfort, A. Berkani, E. Matykina, P. Skeldon, G.E. Thompson, H. Habazaki, K. Shimizu, J. Electrochem. Soc. 152 (2005) C382-C387.

[4] A.A. Voevodin, A.L. Yerokhin, V.V. Lyubimov, M.S. Donley, J.S. Zabinski, Surf. Coat. Technol. 86-87 (1996) 516-521.

[5] S.V. Gnedenkov, O.A. Khrisanfova, A.G. Zavidnaya, S.L. Sinebrukhov, P.S. Gordienko, S. Iwatsubo, A. Matsui, Surf. Coat. Technol. 145 (2001) 146-151.

[6] L. Rama Krishna, K.R.C. Somaraju, G. Sundararajan, Surf. Coat. Technol. 163-164 (2003) 484-490.

[7] X. Nie, E.I. Meletis, J.C. Jiang, A. Leyland, A.L. Yerokhin, A. Matthews, Surf. Coat. Technol. 149 (2002) 245-251.

[8] P. Gupta, G. Tenhundfeld, E.O. Daigle, D. Ryabkov, Surf. Coat. Technol. 201 (2007) 8746-8760.

[9] M.D. Klapkiv, H.M. Nykyforchyn, V.M. Posuvailo, Mater. Sci. 30 (1995) 333-343.

[10] F. Mécuson, T. Czerwiec, T. Belmonte, L. Dujardin, A. Viola, G. Henrion, Surf. Coat. Technol. 200 (2005) 804-808.

[11] F. Mécuson, PhD thesis, Institut National Polytechnique de Lorraine, Nancy (2005) (in French)

[12] R. Arrabal, E. Matykina, T. Hashimoto, P. Skeldon, G.E. Thompson, Surf. Coat. Technol. 203 (2009) 2207-2220.

[13] C.S. Dunleavy, I.O. Golosnoy, J.A. Curran, T.W. Clyne, Surf. Coat. Technol. 203 (2009) 3410-3419.

[14] S. Stojadinović, R. Vasilić, I. Belča, M. Petković, B. Kasalica, Z. Nedić, Lj. Zeković, Corros. Sci. 52 (2010) 3258-3265.

[15] J. Jovović, S. Stojadinović, N.M. Šišović, N. Konjević, Surf. Coat. Technol. 206 (2011) 24-28

[16] S. Stojadinović, M. Perić, M. Petković, R. Vasilić, B. Kasalica, I. Belča, J. Radić- Perić Electrochimica Acta 56 (2011) 10122-10129

[17] J. Jovović, S. Stojadinović, N.M. Šišović, N. Konjević, Journal of Quantitative Spectros. Radiative Transfer 113 (2012) 1928-1937

[18] A.L. Yerokhin, L.O. Snizhko, N.L. Gurevina, A. Leyland, A. Pilkington, A. Matthews, Surf. Coat. Technol. 177-178 (2004) 779-783.

[19] E. Matykina, A. Berkani, P. Skeldon, G.E. Thompson, Electrochimica Acta 53 (2007) 1987-1994.

[20] F. Jaspard-Mécuson, T. Czerwiec, G. Henrion, T. Belmonte, L. Dujardin, A. Viola, J. Beauvir, Surf. Coat. Technol. 201 (2007) 8677-8682.

[21] A. Melhem, G. Henrion, T. Czerwiec, J.L. Briançon, T. Duchanoy, F. Brochard, T. Belmonte, Surf. Coat. Technol. 205 (2011) S133-S136.

[22] A. Melhem, PhD thesis, Institut National Polytechnique de Lorraine, Nancy (2011) (in French).

[23] A.L. Yerokhin, A. Shatrov, V. Samsonov, P. Shashkov, A. Pilkington, A. Leyland, A. Matthews, Surf. Coat. Technol. 199 (2005) 150-157.

[24] P. Bala Srinivasan, J. Liang, R.G. Balajeee, C. Blawert, M. Störmer, W. Dietzel, Appl. Surf. Sci. 256 (2010) 3928-3935.

[25] J. Beauvir, Patent WO 01/81658 A1 (2001).

[26] S. Bardin, J-L. Briancon, F. Brochard, V. Martin, Y. Zayachuk, R. Hugon, J. Bougdira, Contrib. Plasma Phys. 51 (2011) 246-251.

[27] Y. Zayachuk, F. Brochard, S. Bardin, J.L. Briançon, R. Hugon, J. Bougdira, submitted to Rev. Sci. Instrum. arXiv:1010.3432v1 (2010).

[28] A. Melhem, F. Brochard, G. Henrion, J.L. Briançon, T. Czerwiec, T. Belmonte, 63rd Gaseous Electronic Conference (GEC) and 7th Int. Conf. Reactive Plasmas (2010) Paris.

Tables

Table 1: Chemical composition of 2214 and 1050 Al alloys (wt. %)

Al grade	Al	Cu	Mg	Mn	Fe	Si	Zn	Ti	Cr
Al 2214	balance	3.9-5	0.5-1.2	0.4-1.2	0.3	0.5-1.2	0.25	0.15	0.1
Al 1050	balance	0.05	0.05	0.05	0.4	0.25	0.07	0.05	-

List of figure captions

Figure 1: Variation of the anodic current and voltage over the process time for Al2214 alloy sample processed with J_p = 88.4 A.dm^{-2} and F = 100 Hz. The vertical dash line corresponds to the "arc" to "soft" regime switching time

Figure 2: "Arc" to "soft" regime switching time as a function of a) the current density J_p (for Al2214 alloy sample processed with F = 100 Hz) and b) the current pulse frequency F (for Al1050 alloy sample processed with J_p = 75.7 A.dm^{-2})

Figure 3: Pictures of the spatial distribution of micro-discharges events over the surface of the Al1050 alloy sample processed with J_p = 75.5 A.dm^{-2} and F = 100 Hz at various stages: a) 1 min; b) 5 min; c) 10 min and d) 15 min. Each picture corresponds to the integration of 11250 successive images recorded over 90 ms (9 pulse periods)

Figure 4: Micro-discharges surface number density as a function of the PEO process time for various a) current densities J_p (for Al2214 alloy sample processed with F = 100 Hz) and b) current pulse frequencies F (for Al1050 alloy sample processed with J_p = 75.7 A.dm^{-2})

Figure 5: Lifetime distribution of micro-discharges recorded at 10 min processing time (before "soft" sparking regime) for various a) current densities J_p (for Al2214 alloy sample processed with F = 100 Hz) and b) current pulse frequencies F (for Al1050 alloy sample processed with J_p = 75.7 A.dm^{-2})

Figure 6: Size distribution of micro-discharges recorded at 10 min processing time (before "soft" sparking regime) for various a) current densities J_p (for Al2214 alloy sample processed with F = 100 Hz) and b) current pulse frequencies F (for Al1050 alloy sample processed with J_p = 75.7 A.dm^{-2})

Figure 7: Backscattered electron micrographs of the cross-sections of PEO processed samples:

a) Al2214 – 100 min – 12.6 A.dm^{-2} – 100 Hz – At the centre of the sample
b) Al2214 – 100 min – 12.6 A.dm^{-2} – 100 Hz – At the edge of the sample

c) Al1050 – 40 min – 75.5 A.dm^{-2} – 100 Hz – At the centre of the sample
d) Al1050 – 40 min – 75.5 A.dm^{-2} – 100 Hz – At the edge of the sample
e) Al1050 – 40 min – 75.5 A.dm^{-2} – 900 Hz – At the centre of the sample
f) Al1050 – 40 min – 75.5 A.dm^{-2} – 900 Hz – At the edge of the sample

Figure 8: Dependence of the average growth rate of the oxide layer at the centre and the edge of PEO processed samples on a) the current density J_p (for Al2214 alloy sample processed with F = 100 Hz, after 70 min treatment) and b) the current pulse frequency F (for Al1050 alloy sample processed with J_p = 75.7 A.dm^{-2} , after 40 min treatment)

Figure 9: Dependence of the roughness of the oxide layer at the centre and the edge of PEO processed samples on a) the current density J_p (for Al2214 alloy sample processed with F = 100 Hz, after 70 min treatment) and b) the current pulse frequency F (for Al1050 alloy sample processed with J_p = 75.7 A.dm^{-2} , after 40 min treatment)

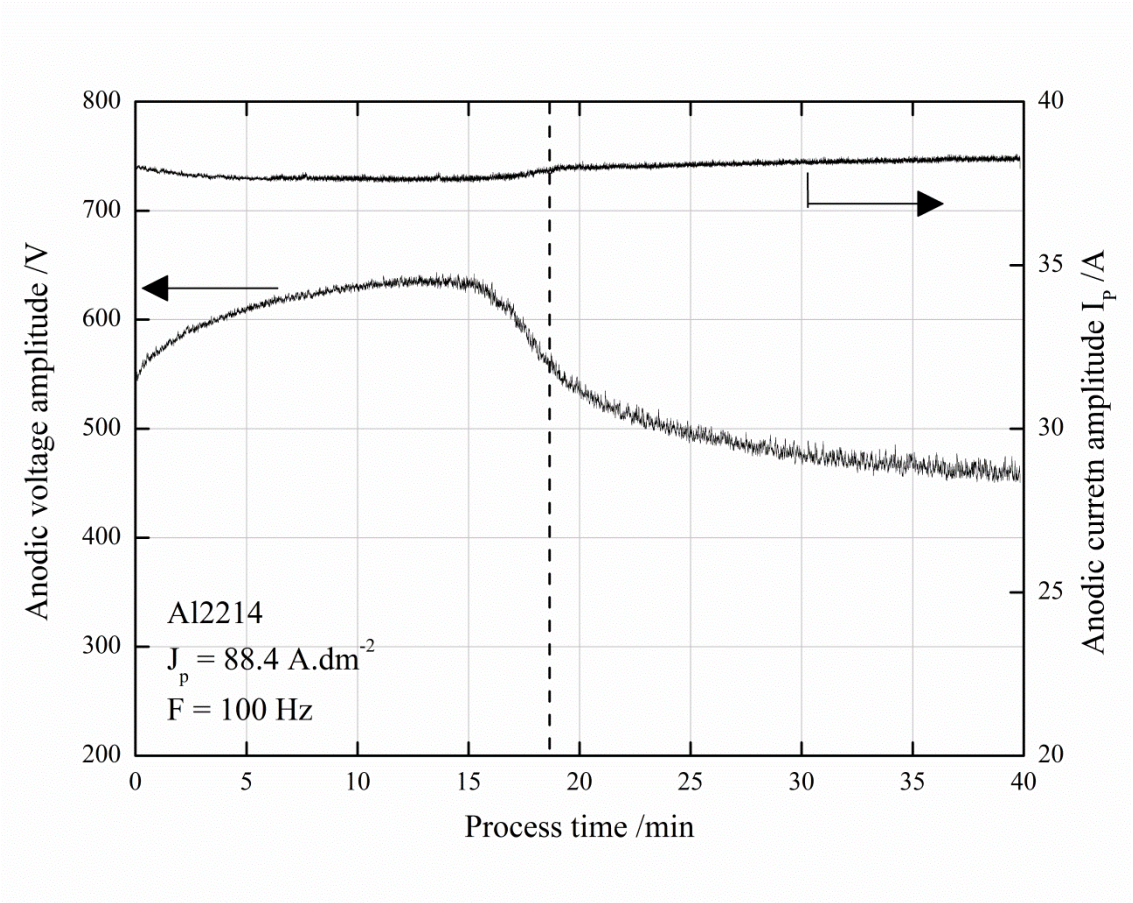
Anodic voltage amplitude /V
Anodic curretn amplitude I_p /A
Process time /min
Al2214
J_p = 88.4 A.dm^{-2}
F = 100 Hz
800
700
600
500
400
300
200
40
35
30
25
20
0
5
10
15
20
25
30
35
40

Figures 1

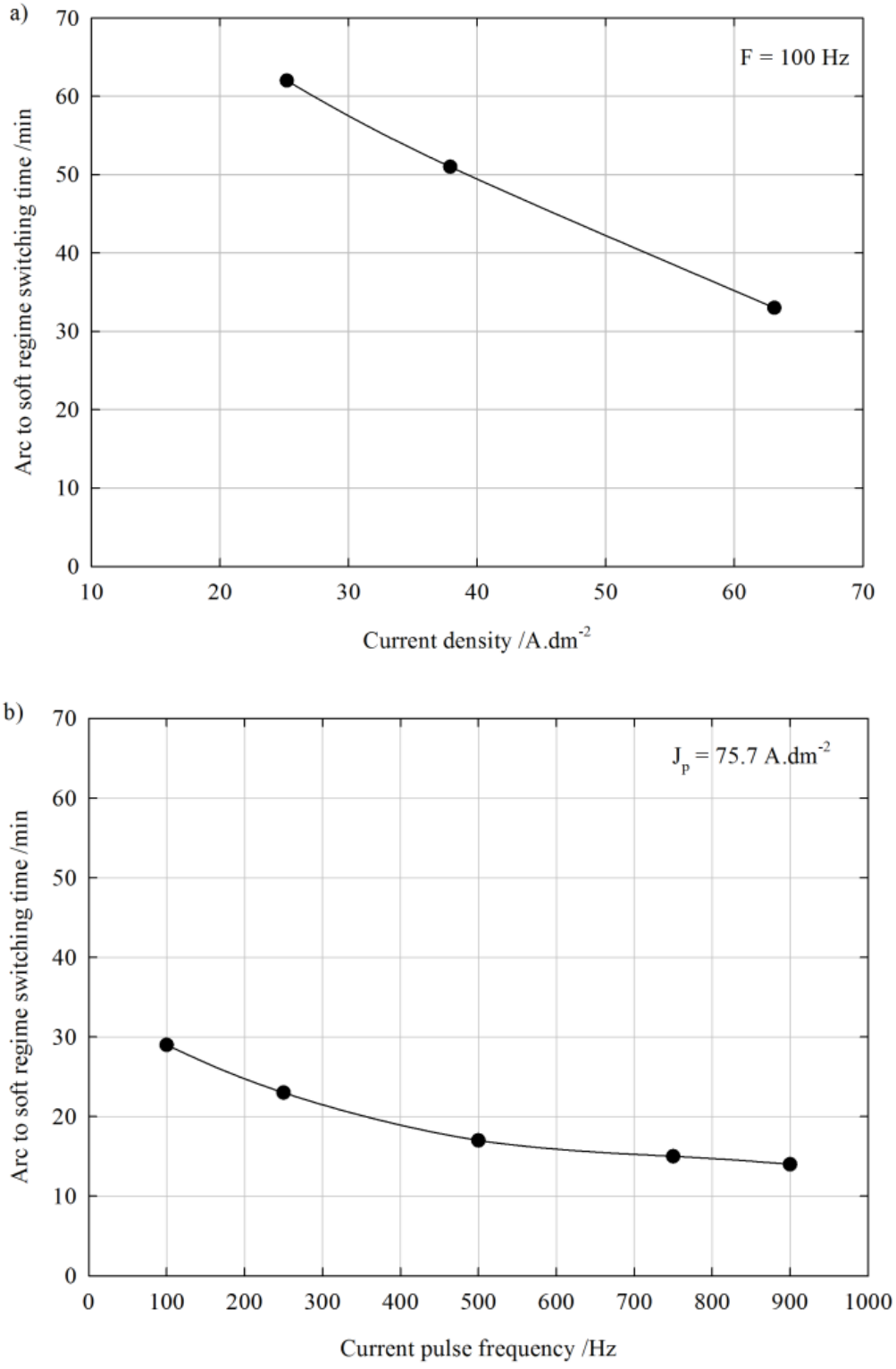
a)
F = 100 Hz
Arc to soft regime switching time /min
Current density /A.dm-2
b)
Jp = 75.7 A.dm-2
Arc to soft regime switching time /min
Current pulse frequency /Hz

Figure 2

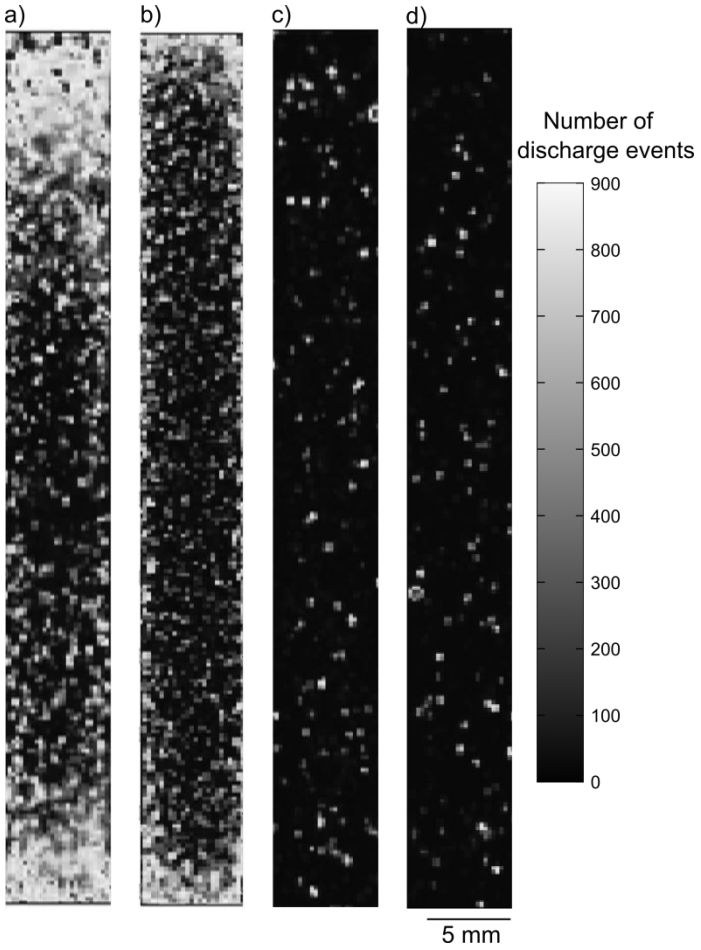
a)
b)
c)
d)
Number of discharge events
900
800
700
600
500
400
300
200
100
0
5 mm

Figure 3

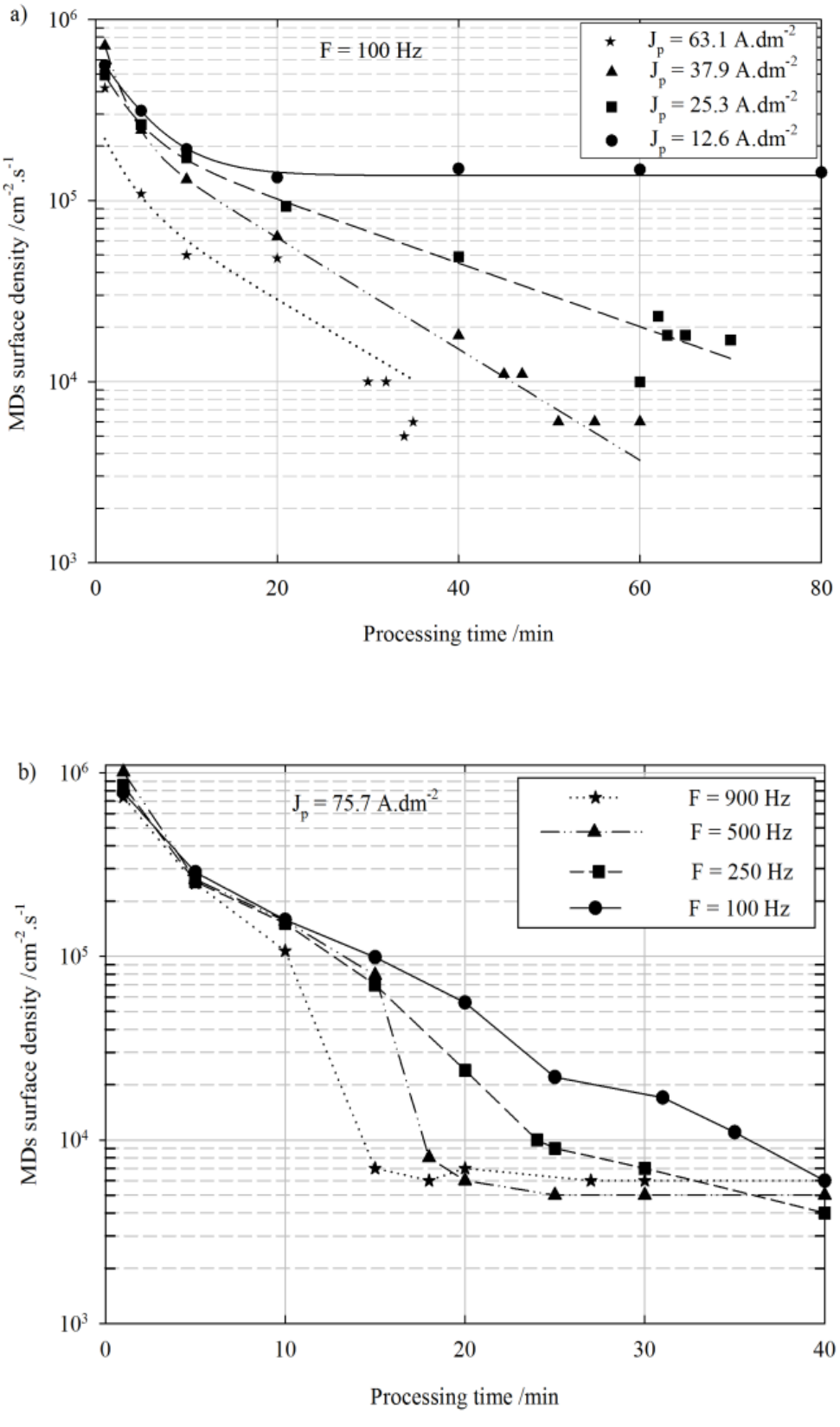
a)
F = 100 Hz
J_p = 63.1 A.dm^{-2}
J_p = 37.9 A.dm^{-2}
J_p = 25.3 A.dm^{-2}
J_p = 12.6 A.dm^{-2}
MDs surface density /cm^{-2}.s^{-1}
Processing time /min
b)
J_p = 75.7 A.dm^{-2}
F = 900 Hz
F = 500 Hz
F = 250 Hz
F = 100 Hz
MDs surface density /cm^{-2}.s^{-1}
Processing time /min

Figure 4

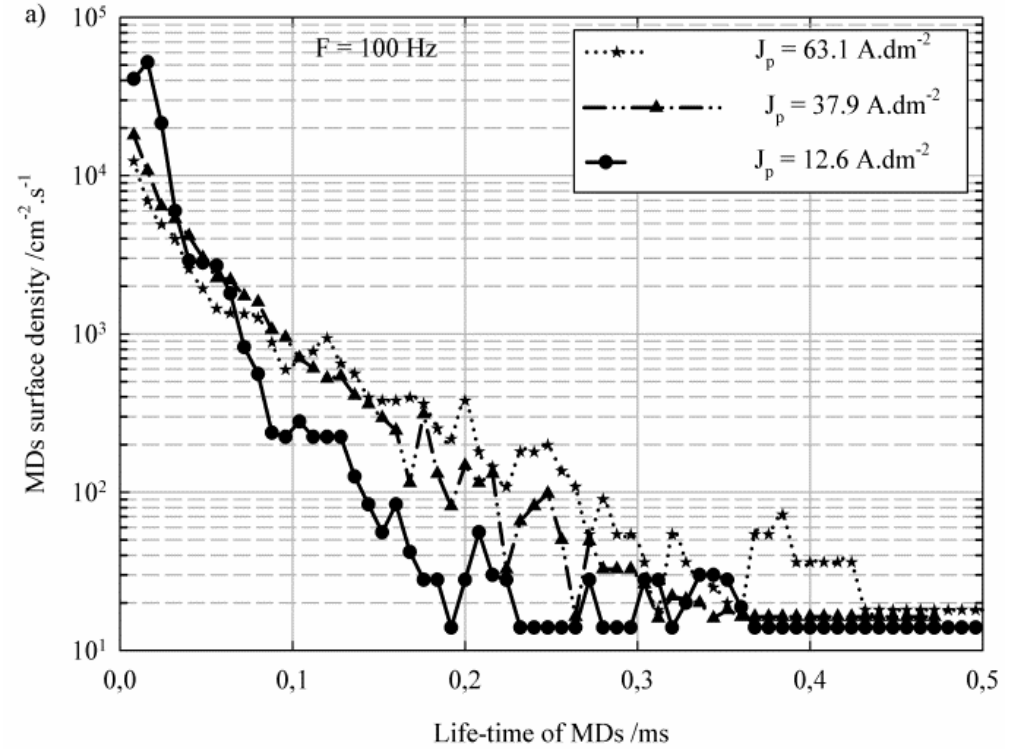
a)
F = 100 Hz
J_p = 63.1 A.dm^{-2}
J_p = 37.9 A.dm^{-2}
J_p = 12.6 A.dm^{-2}
MDs surface density /cm^{-2}.s^{-1}
10^5
10^4
10^3
10^2
10^1
0,0
0,1
0,2
0,3
0,4
0,5
Life-time of MDs /ms

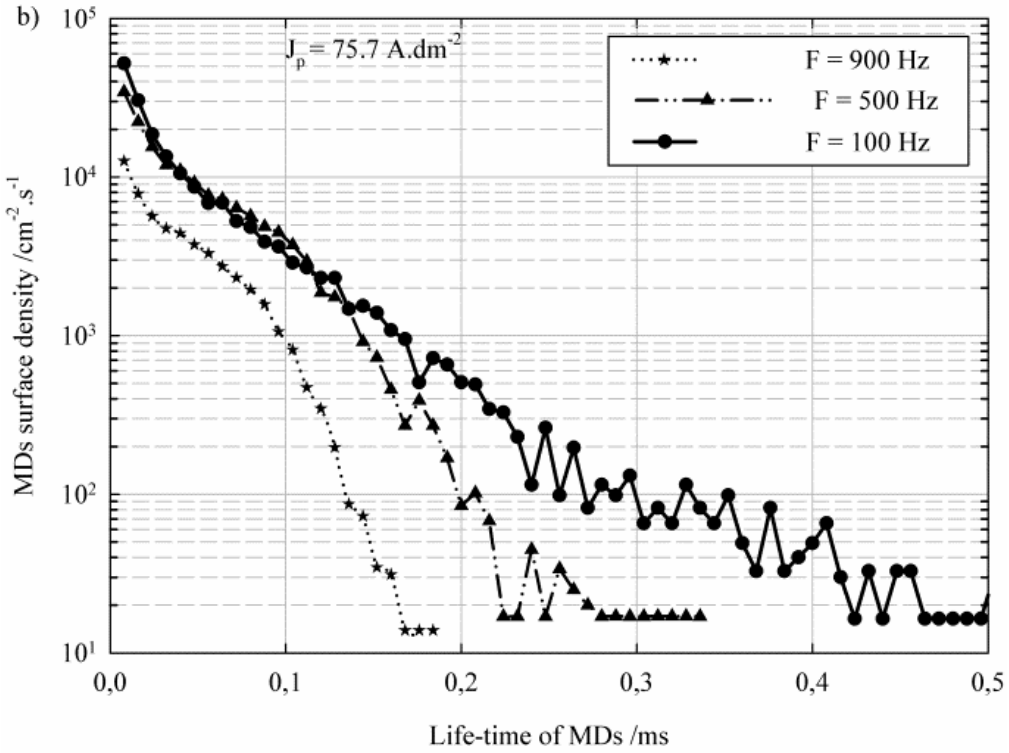
b)
J_p = 75.7 A.dm^{-2}
F = 900 Hz
F = 500 Hz
F = 100 Hz
MDs surface density /cm^{-2}.s^{-1}
10^5
10^4
10^3
10^2
10^1
0,0
0,1
0,2
0,3
0,4
0,5
Life-time of MDs /ms

Figure 5

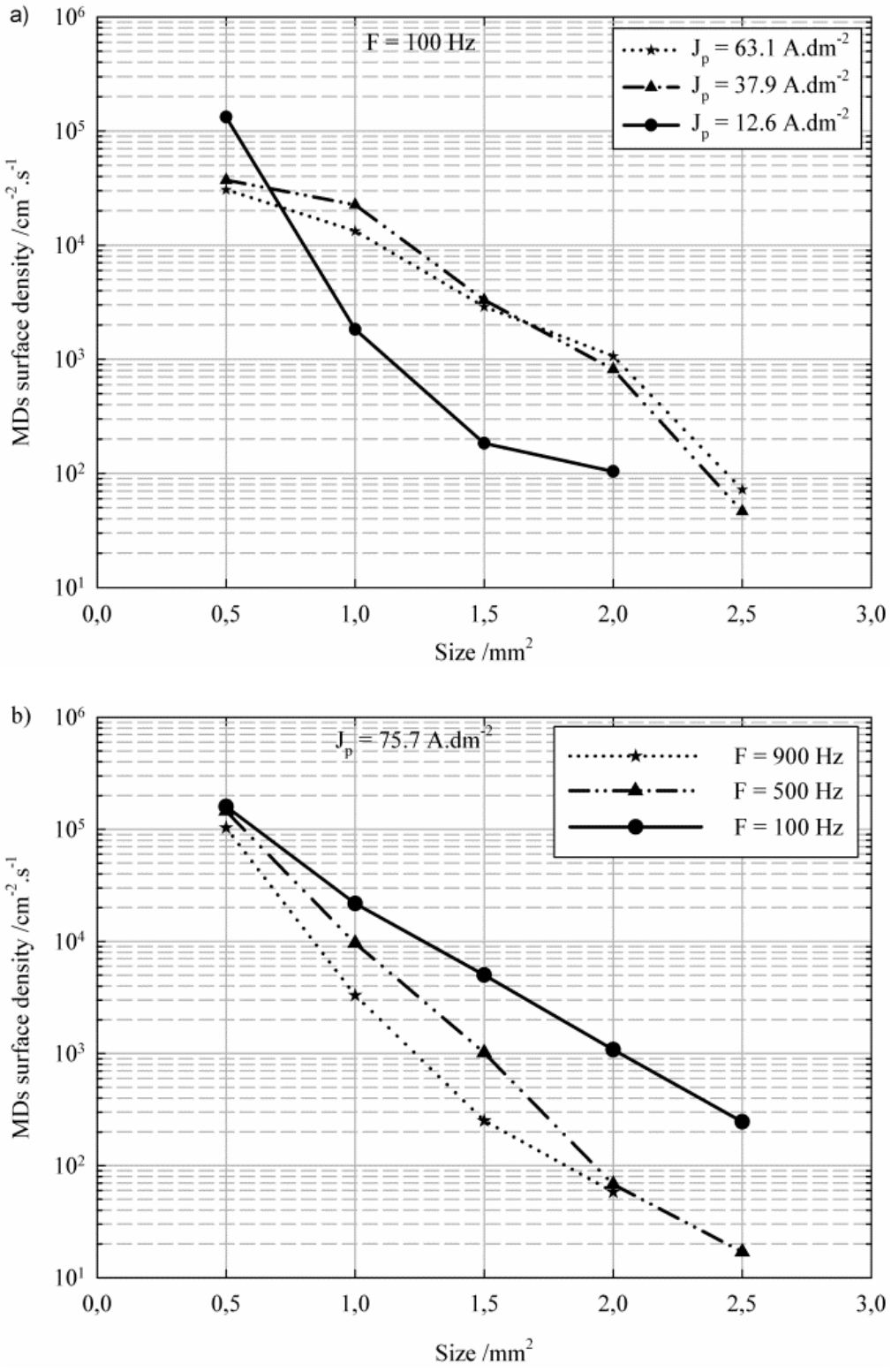
a)
F = 100 Hz
J_p = 63.1 A.dm^{-2}
J_p = 37.9 A.dm^{-2}
J_p = 12.6 A.dm^{-2}
MDs surface density /cm^{-2}.s^{-1}
Size /mm^2
b)
J_p = 75.7 A.dm^{-2}
F = 900 Hz
F = 500 Hz
F = 100 Hz
MDs surface density /cm^{-2}.s^{-1}
Size /mm^2

Figure 6

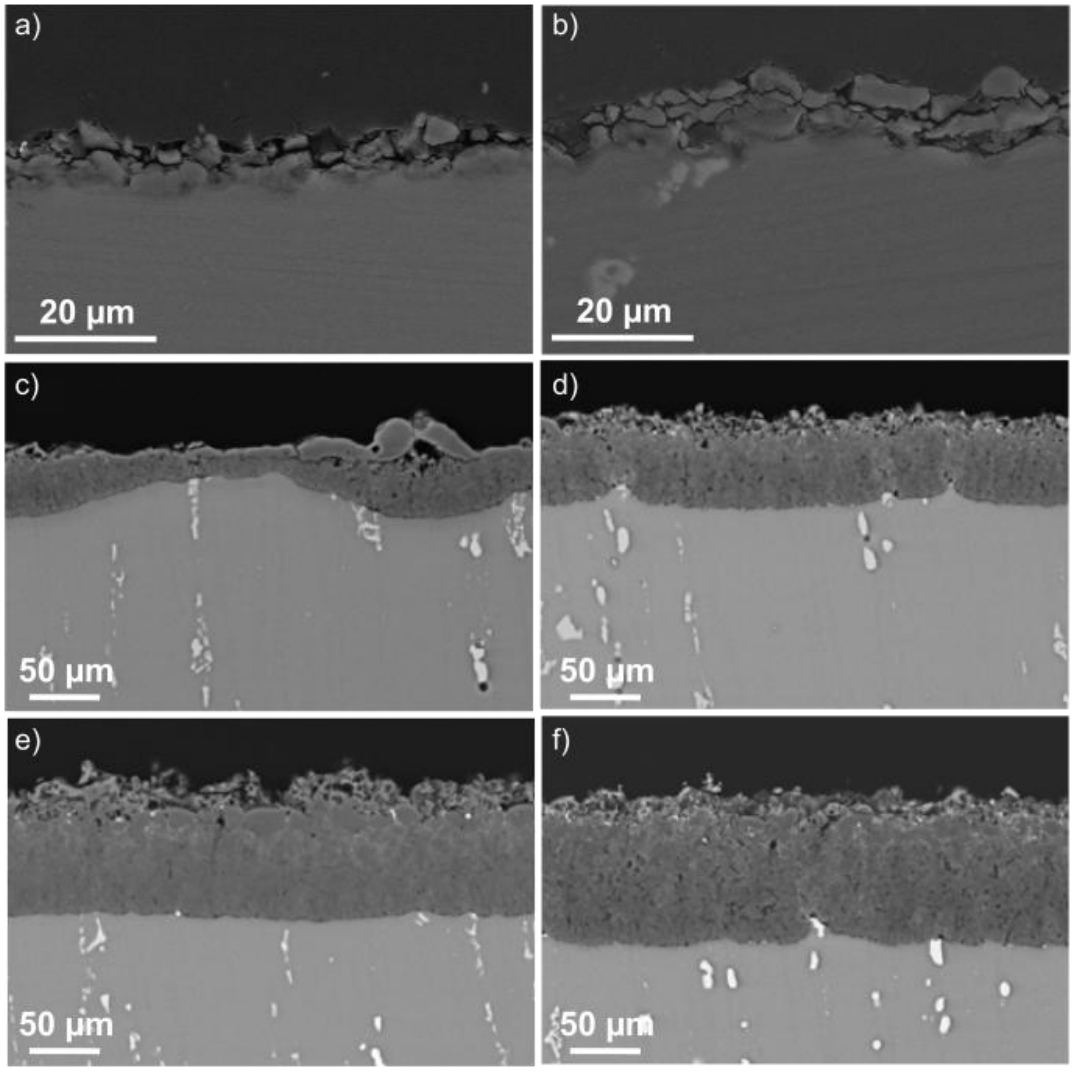

Figure 7

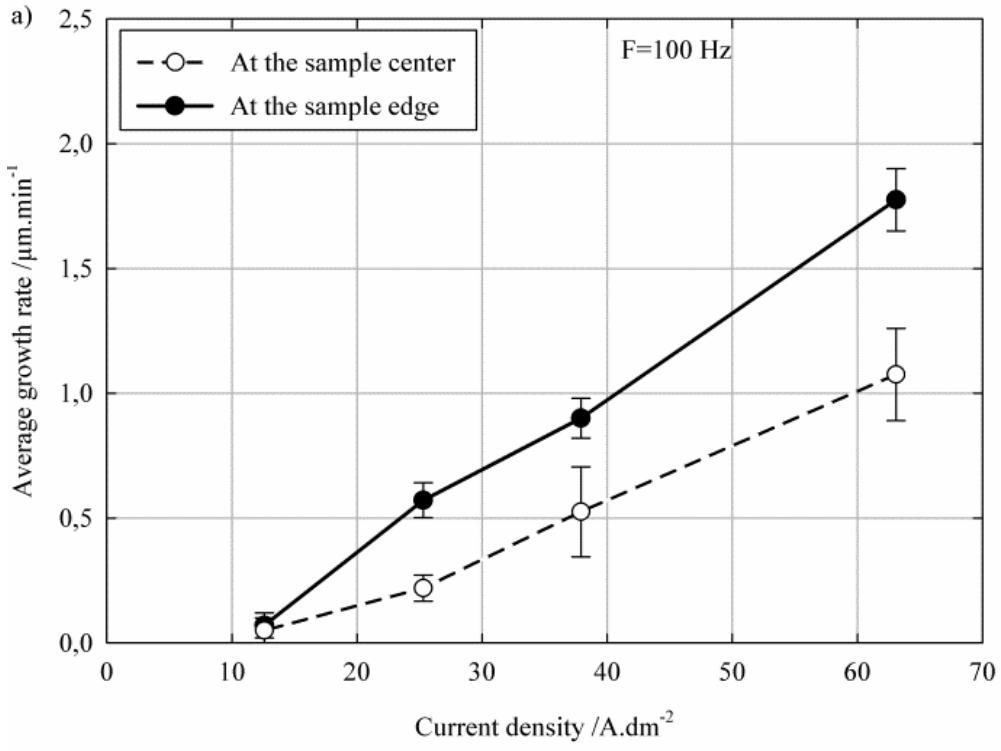
a)
At the sample center
At the sample edge
F=100 Hz
Average growth rate /µm.min-1
Current density /A.dm-2
0,0
0,5
1,0
1,5
2,0
2,5
0
10
20
30
40
50
60
70

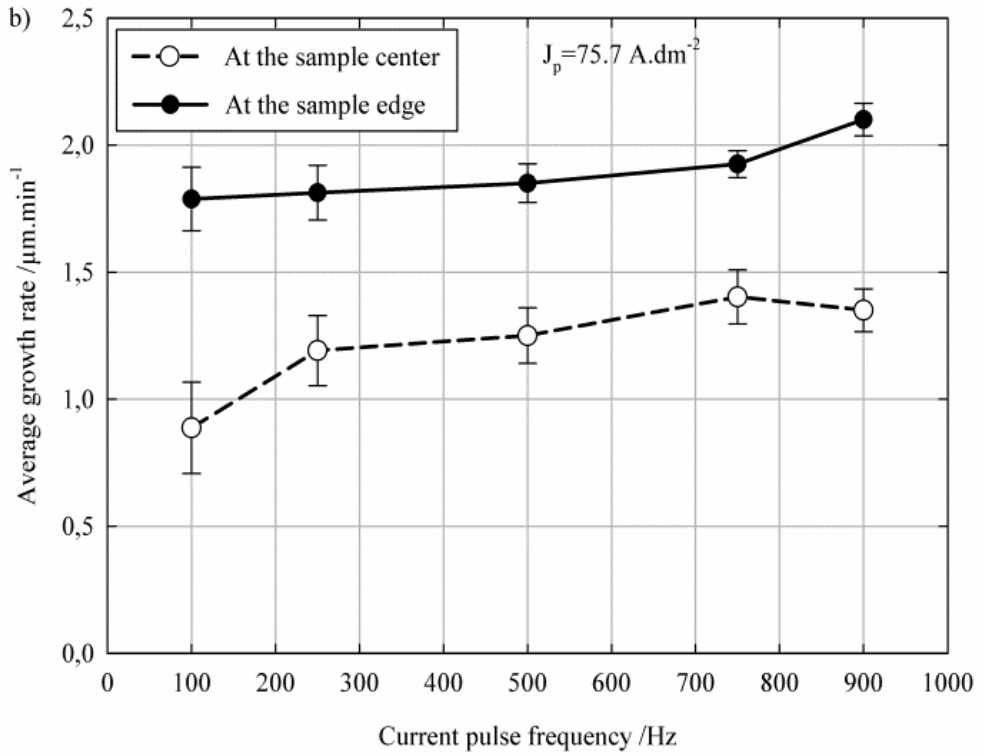
b)
At the sample center
At the sample edge
Jp=75.7 A.dm-2
Average growth rate /µm.min-1
Current pulse frequency /Hz
0,0
0,5
1,0
1,5
2,0
2,5
0
100
200
300
400
500
600
700
800
900
1000

Figure 8

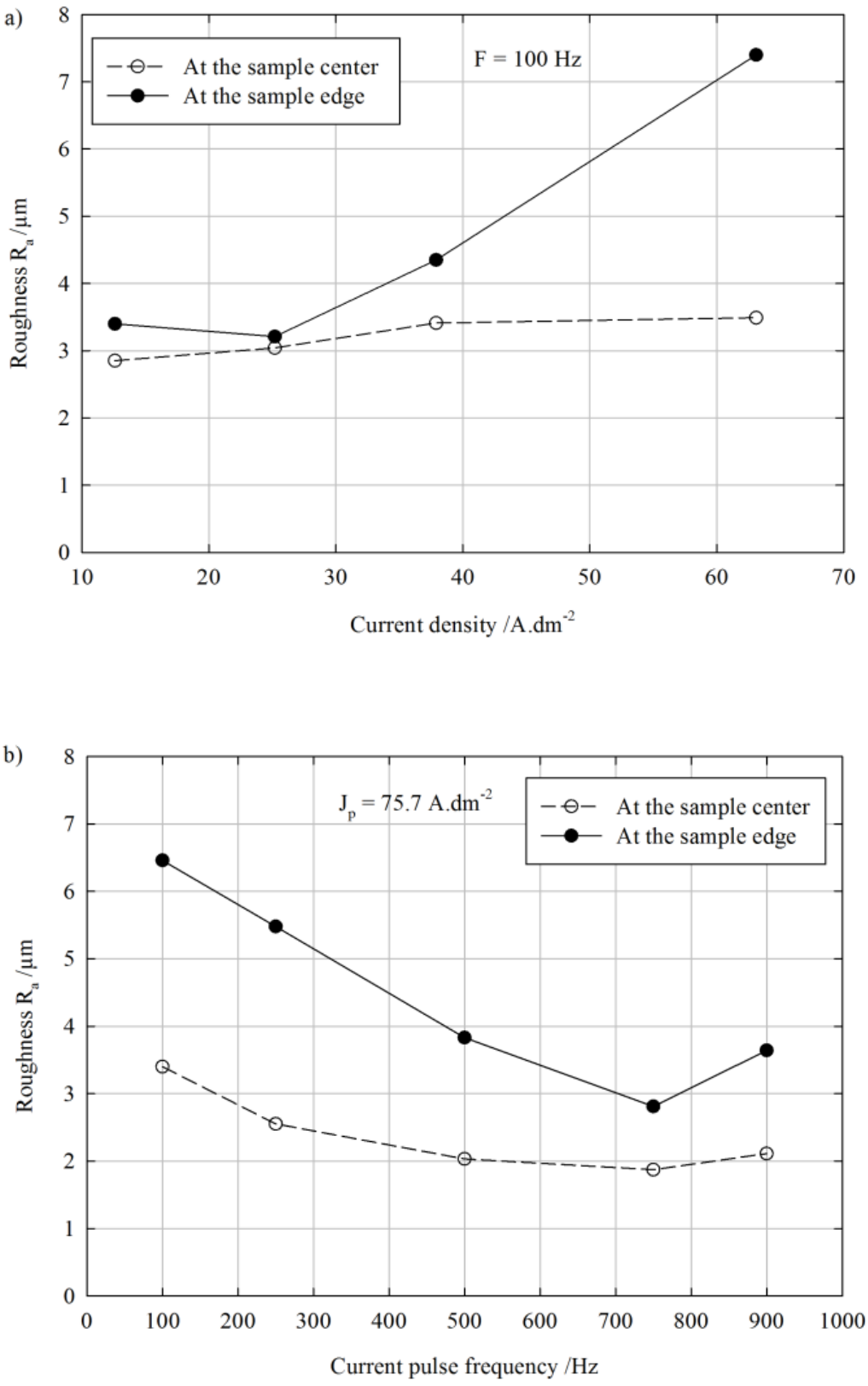
a)
At the sample center
At the sample edge
F = 100 Hz
Roughness R_a /µm
Current density /A.dm^{-2}
b)
J_p = 75.7 A.dm^{-2}
At the sample center
At the sample edge
Roughness R_a /µm
Current pulse frequency /Hz

Figure 9